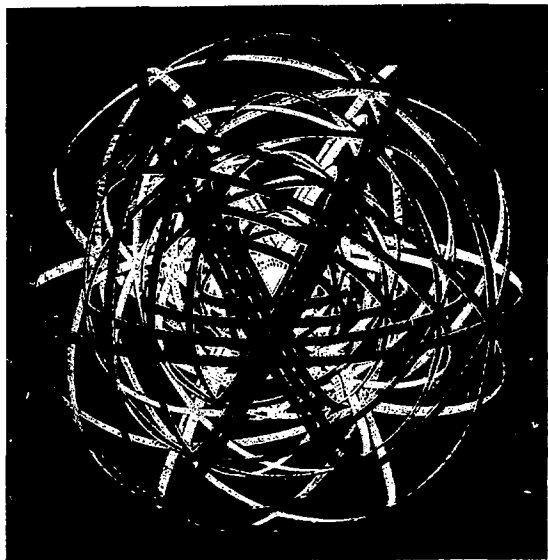


FR 8403284

LPNHE\_83-07

LPNHE\_Paris 83-07



Production inclusive de  $\Lambda$  et de  $\bar{\Lambda}$  dans les annihilations  
 $e^+ e^-$  à 29 GeV.

par Christian de la Vaissière

BIBLIOTHÈQUE SACLAY  
LE 25 JUIN 1984

ERRATUM

Avant-propos, 3<sup>e</sup> paragraphe : lire 2.0 GeV/c au lieu de 0.5 GeV/c.

## AVANT-PROPOS

---

Le travail qui suit étant à l'origine un rapport interne de l'expérience MARK II, destiné à fournir les bases d'une publication , il est apparu nécessaire de le faire précéder d'un avant propos explicatif.

Les laboratoires impliqués dans l'expérience sont SLAC, le Lawrence Berkeley Laboratory et Harward. Cette collaboration prend actuellement des données sur les anneaux de collision  $e^+e^-$  PEP du SLAC. L'énergie des collisions est de 29 GeV.

Le sujet de l'étude est la production inclusive des  $\Lambda$  et  $\bar{\Lambda}$  dans les annihilations  $e^+e^- \rightarrow$  hadrons. Son intérêt est de fournir des données sur les conditions dans lesquelles les baryons sont produits dans le processus d'hadronisation de la paire  $q\bar{q}$  primaire. Ce phénomène reste mal connu. L'hyperon  $\Lambda$  possède l'avantage sur le proton de pouvoir être identifié pratiquement sans ambiguïté, grâce à sa désintégration, pratiquement dans tout le domaine d'impulsion (MARK II n'identifie les protons par temps de vol qu'en dessous de 0.5 GeV/c). Les  $\Lambda$  (et  $\bar{\Lambda}$ ) constituent donc des particules idéales pour sonder la production de baryons dans les jets hadroniques.

De tous les détecteurs actuellement en place sur PETRA et PEP, MARK II est le mieux placé pour une telle étude. Son atout principal est une chambre à dérive de haute précision (appelée "Vertex chamber" (VC)) installée depuis décembre 1981. Ce détecteur de vertexs secondaires qui voit la zone la plus proche du point d'interaction s'est avéré un outil remarquable pour la mesure de très courtes vies moyennes ( $t, D^\circ, b$ ) et la reconnaissance de  $K^\circ$  et de  $\Lambda^\circ$ s. Par ailleurs la campagne de prises de données 1982/83 a coïncidé avec un fonctionnement remarquable de la machine PEP permettant d'accumuler 4 fois plus de données que lors du cycle précédent. La luminosité totale ainsi obtenue

(133.6 evt/eb, soit pour une section efficace hadronique de 0.4 nb, environ 53000 évènements) donne à l'expérience MARK II l'avantage d'une statistique supérieure à celles d'autres groupes.

Les premières données concernant la production de  $\Lambda$  ont été fournies par TASSO à PETRA. Le nombre de  $\Lambda$  et  $\bar{\Lambda}$  sur lequel est basé cette étude est grossso modo le double de celui de TASSO, mais l'avantage décisif provient de ce que le détecteur de vertex permet de disposer d'un lot de  $\Lambda/\bar{\Lambda}$  beaucoup moins contaminés.

Ce rapport utilisant quelques notations propres à l'expérience et faisant référence à des documents internes difficilement accessibles, des notes explicatives ont été ajoutées, ainsi que deux annexes donnant une description sommaire du détecteur et un extrait d'un rapport précédent introduisant la notion de qualité d'un V°.

SLAC MEMORANDUM

November 2, 1983

To: PEP-5 Collaboration  
 From: Ch. de la Vaissiere, Drew Baden  
 Subject: Status report on  $\Lambda$  analysis

---

Introduction

A large amount of data has been accumulated since the early report written in march 1983<sup>1</sup>. The large statistics now available allow one to go beyond the measurement of inclusive cross-sections. Unfortunately, the inefficiencies of the drift chamber during the last cycle are not yet well understood, and so a large fraction of the data cannot be fully used.

Data sample

This survey is based on an integrated luminosity of  $133.6 \text{ pb}^{-1}$ . It includes the data accumulated with the vertex chamber during the 1981/1982 cycle (VCSUM SUMMARY)<sup>2</sup> and the 1982/1983 cycle ( runs 9939-11472). The  $15 \text{ pb}^{-1}$  of data without the vertex chamber (29GEV SUMMARY) have not been used for this analysis. The gain in statistical accuracy has become marginal compared to the inconveniences due to the handling of data taken with a different apparatus. Furthermore, the  $\Lambda$  signal/background ratio is poor compared to the one obtained with the vertex chamber.

Among the  $114.3 \text{ pb}^{-1}$  accumulated during the last cycle,  $88.4$  have suffered from the drift chamber problems<sup>(xx)</sup>. The remaining  $25.7 \text{ pb}^{-1}$  (runs 11107-11472), corresponding to the period where oxygen has been added to the drift chamber gas, have been compared with the data of the previous cycle(VCSUM). The raw number of  $\Lambda$ 's /  $\text{pb}^{-1}$  have been found to be  $9.3 \pm 0.9$  and  $8.5 \pm 0.8$  respectively. If one divides the momentum spectrum in 7 intervals, the two samples normalized to luminosities agrees with a  $\chi^2$  of 6 for 7 degrees of freedom. Therefore, we have added VCEUM and OXYGEN into a "good data" sample of  $45.2 \text{ pb}^{-1}$ .

We have also compared the rest of the data to this reference sample. The ratio of the  $\Lambda$  yields is found to be  $0.776 \pm 0.050$ , significantly lower than 1. A comparison made at the level of the  $\Lambda$  momentum distributions indicates that the inefficiency does not vary in first approximation with  $P_\Lambda$ : taking into account a global 0.776 ratio, the  $\chi^2$  is  $7.8/6$ .

The determination of the cross-sections has been based on the good data sample. For the other topics the whole sample has been considered.

<sup>(x)</sup> VCSUM SUMMARY est le nom du fichier contenant les données prises en 1981/1982 ( $13.6 \text{ pb}^{-1}$ ) première année de fonctionnement de la chambre de haute précision; 29 GeV SUMMARY celui des données prises sans cette chambre, non utilisées pour cette étude.

Pendant une partie de l'année 1982/83 la chambre à dérive principale de MARK II a fonctionné avec une efficacité réduite. Le fichier OXYGEN correspond à la période durant laquelle l'efficacité a été égale à celle de l'année précédente.

Event and  $\Lambda$  selection

The selection of hadronic events is:

NCHARG	> 5
E CODE	> 3
ZVT	< 5 cm

The selection of the  $\Lambda$  and  $\bar{\Lambda}$  has been detailed in previous reports<sup>1,2</sup>.

1) First the vertex finder package VFINDP<sup>3</sup> is used to select and reconstruct candidates  $K^0$  and  $\Lambda^0$ 's. The  $\Lambda$  and  $\bar{\Lambda}$  cuts are: ~~xx~~

Distance of closest approach to the interaction point,

$\pi$	> 2 mm
p	> 1 mm
$\Lambda$	< 5 mm

Match in z of secondaries at secondary vertex ~~xxx~~ < 5 cm

Distance of closest approach in z of secondaries < 10 cm

$c\tau(\Lambda)$	> 4 mm
------------------	--------

$\chi^2$ of V geometrical fit (1-c)	< 10.
-------------------------------------	-------

Fitted mass of V	[1.092, 1.1140] GeV
------------------	---------------------

This set of cuts is soft, and optimized to remove background at the cost of a minimum loss of signal.

2) A large fraction of the remaining background is removed through a quality cut. This  $\Lambda$  quality has been defined in a previous note<sup>2</sup>. We use the standard cut: QUALB4( $\Lambda$ )=-1.50. The removal of background due to the quality cut appears very clean on fig. 1.b. ~~xxxx~~

3) In order to remove regions of low acceptance, we required finally that:

$ \cos(\theta(\Lambda)) $	< 0.75
$c\tau(\Lambda)$	> 1 cm.

The final  $\Lambda/\bar{\Lambda}$  sample is shown Fig.1. It contains around 955  $\Lambda$  or  $\bar{\Lambda}$  in the mass range [1.102, 1.126] with a signal/background ratio of  $\approx 5.5$ . In the following the term  $\Lambda$  will refer to both  $\Lambda$  and  $\bar{\Lambda}$ . The subtraction of the background below the  $\Lambda$  is made by a peak minus wing subtraction.

mass resolution

The statistics allows us to measure the variation of the mass resolution with momentum. The resolution increases from  $\approx 3$  MeV for slow  $\Lambda^0$ 's to above 7 MeV for fast  $\Lambda^0$ 's. This variation agrees with the Monte-Carlo predictions (Fig.2).

(\*) Il s'agit d'une sélection standard d'événements hadroniques

(\*\*) VFINDP est décrit sommairement en annexe

(\*\*\*) La reconstruction des traces en z (le long de l'axe du faisceau)

est beaucoup plus imprécise que dans le plan x,y perpendiculaire à cet axe.  
(\*\*\*\*) Voir annexe.

Inclusive cross-sections

The limited sample of  $45.2 \text{ pb}^{-1}$  has been used for this study. 13678 events pass the hadronic cuts. The raw number of  $\Lambda/\bar{\Lambda}$  is  $404 \pm 24$ .<sup>x</sup> The efficiency is calculated from the Monte-Carlo events that use BCQCD as a generator. The efficiency is 0 below  $0.5 \text{ GeV}/c$ . It reaches a maximum of 12% at  $1.5 \text{ GeV}/c$  and decreases slowly to around 7% at  $7 \text{ GeV}/c$ . The inclusive cross section corrected for acceptance is shown in Fig.3-a. This estimation is based on the luminosity coming out of Bhabha events. Radiative corrections have not been applied. It can be seen that the  $\Lambda^0$ 's are sensibly softer in the BCQCD model than in the data.  $\Lambda$  production is also overestimated by 40%. In the Fig.3-b the invariant cross-section  $s/0 \frac{d\sigma}{dx_\Lambda}$  is compared to previous results by TASSO<sup>5</sup> and JADE<sup>6</sup>. JADE is able to explore slow  $\Lambda^0$ 's, while TASSO has access to a momentum range similar to ours. Both experiments are well below our present statistical accuracy.

The inclusive  $\Lambda$  cross section agrees in shape and magnitude with the early measurements, except maybe in the range of high  $x$  values where both statistical and systematical errors are large. In the Fig.4, we have added data coming from the sample with drift chamber inefficiencies, giving them a weight  $1/0.776$  independent of momentum.

The total cross-section in the range  $P_\Lambda > 0.5 \text{ GeV}/c$  is  $87.6 \pm 5.2 \pm 6.0 \text{ pb}$ . The correction for  $\Lambda$  below  $0.5 \text{ GeV}/c$  is estimated to 3%, and the corrected value is

$$\sigma_\Lambda = 90.2 \pm 5.4 \pm 6.0 \text{ pb}$$

Most of the systematical error comes from the uncertainty in the luminosity. The ratio  $R_\Lambda$  of the cross-section to  $\sigma_{\mu\mu}$  is  $0.87 \pm 0.05 \pm 0.06$  and the number of  $\Lambda$  and  $\bar{\Lambda}$  per hadronic event is  $0.22 \pm 0.013$ . This should be compared to the value of  $R_\Lambda$  given by TASSO at  $33 \text{ GeV}$ ,  $1.12 \pm 0.15 \pm 0.17$  and to our early measurement of 1981<sup>4</sup>,  $.80 \pm 0.24$ .

If instead of normalizing the number of  $\Lambda^0$ 's to the Bhabha luminosity, the total number of hadronic events is used, the  $\Lambda$  cross-section is found to be  $81. \pm 5.0 \text{ pb}$ .

Baryon-antibaryon correlations

Baryon-antibaryon correlations are interesting since they can shed some light to poorly understood features: How baryons are produced in jets? Is the baryon number conserved locally? Do some jets carry leading diquarks? The advantage of using  $\Lambda^0$ 's is that they can be detected over a fairly broad range of momentum. Protons and antiprotons rely on the time-of-flight and can be identified only below  $2 \text{ GeV}/c$ .

 $\Lambda-\bar{\Lambda}$  correlations

11  $\Lambda\bar{\Lambda}$  events were found after quality cuts compared to 5 compatible with  $\Lambda\Lambda$  or  $\bar{\Lambda}\bar{\Lambda}$ . The 2-dimensional mass plot of  $\Lambda\bar{\Lambda}$  events suggests that these

(\*) Il n'existe pas de modèle satisfaisant pour la production de baryons, celle-ci est introduite empiriquement, sous forme de probabilités de production de diquarks, dans le processus d'hadrionisation. BCQCD est une version du programme JETSET, Fleischman et Wiedner avec une hadronisation à la Feynman et Field. BCQCD est principalement utilisée ici pour calculer l'acceptance.

events are genuine associated production(fig.5). The low statistics allow only a classification between pairs belonging to the same or opposite jet. This gives:

	same jet	opposite jet
$\Lambda\bar{\Lambda}$	6	5
$\Lambda\Lambda + cc.$	4	1

An individual display of these few events shows than none of the 5  $\Lambda\bar{\Lambda}$  pairs in opposite jets are compatible with a hypothesis of a leading diquark. Most of them are soft

#### $\Lambda\text{-}\bar{B}$ and $\bar{\Lambda}\text{-}p$ correlations:

$p$  and  $\bar{p}$  were defined by the conditions: (\*)

$p$	$< 2.0 \text{ GeV}$
$WPR$	$> 0.70$
$TQUAL$	$= 1 \text{ or } 2$

The cosine of the angle between a  $\Lambda$  and a  $\bar{p}$  (or a  $\bar{\Lambda}$  and a  $p$ ) is plotted in Fig.6-a. The same angle when both particles have the same baryonic number is plotted on Fig.6-b.  $B=2$  or  $B=-2$  pairs come from events with 2 baryon-antibaryon pairs. We estimate the contribution of single baryon-antibaryon pairs by subtracting the  $|B|=2$  from the  $B=0$  contribution. (fig.7-a) This subtraction indicates that associated baryon-antibaryon pairs belong by a large margin(70/14) to the same jet. Using the same method, it is also meaningful to consider the difference in rapidity along the jet axis between the  $\Lambda$  and the  $\bar{p}$ (fig.7-b). The average  $\Delta Y$  is  $0.83 \pm 0.05$ , significantly less than for the uncorrelated  $B=2$  pairs( $1.62 \pm 0.12$ ). This suggests a dominant local conservation. The Fig.7-c shows  $\Delta\phi$ , the difference in azimuthal angle in the plane perpendicular to the sphericity axis. Here we observe a rather flat distribution which does not show a pronounced peak at  $180^\circ$ . This agrees with a recent result of TASSO<sup>3</sup> on  $p\bar{p}$  correlation and disagrees with a claim made by JADE<sup>4</sup>. We do not observe an angular anti-correlation as predicted for example by the Mayer<sup>5</sup> model.

#### Jet analysis

It was suggested by TASSO<sup>3</sup> that gluon jets fragment more into baryons than do quark jets. We have investigated how  $\Lambda/\bar{\Lambda}$  behave inside jets. We have defined the jet axis with sphericity from JETCAL. Particles used in the jet definition are: 1) the charged particles; 2)  $\gamma$ 's with  $E_T$  above 250 MeV; 3)  $\Lambda^0$ 's and  $K^0$ 's. If  $\Lambda^0$ 's prefer gluons, there should be a difference in sphericity and planarity when a  $\Lambda$  is required or not required in the event. The sphericity and planarity distributions appears fully compatible between the two types of events(fig.8). Comparing now  $\Lambda^0$ 's and charged hadrons in  $\Lambda$  events, it turns out that the  $\Lambda^0$ 's get significantly more  $P_T^2$  (Fig.9). The average value is  $0.83 \pm 0.04$  against  $0.57 \pm 0.01$  for charged

(\*) Ces coupures assurent un échantillon de  $p/\bar{p}$  bien identifiés.

hadrons. This is expected from  $q\bar{q}g$  topologies. When massive particles belong to a jet emitted at a non-zero angle with the primary axis, they will have more transverse momentum than light particles.

We have investigated if, in 3-jets events,  $\Lambda^0$ 's prefer the softer jet which, according to a simulation made by TASSO, is most likely to be the gluon jet(51%). We have followed the TASSO selection of 3 jet events (this calculation uses the reduced momentum  $x$  of the primary partons instead of the observed jet energies). We require in particular that the reduced momentum of the most energetic jet is <0.9 and that the sum of the momenta in each jet is over 1.5 GeV/c. Among the 103  $\Lambda^0$ 's that fell in the 3-jet category, 40 were found to belong to the most energetic jet, 35 to the median jet, and 28 to the softer jet. These results are not acceptance corrected and require further studies. However, there is no striking evidence of a strong relation between  $\Lambda^0$ 's and gluon jets.

#### Fast $\Lambda^0$ 's

Fast  $\Lambda^0$ 's suffer from a poor mass resolution due to the fact that they include high momentum baryons and that they often decay beyond the vertex chamber inner layers. But on the other hand, they are practically background free. Some events containing fast  $\Lambda/\bar{\Lambda}$  have interesting features. The fast  $\Lambda^0$ 's were required to have  $P_\Lambda > 6$  GeV/c. We replaced the condition that the mass belongs to the peak region, by the requirement that the quality is well above the standard quality cut.

In one event (10848/1866), the  $\bar{\Lambda}$  is practically alone in one jet(Fig.9). A second event (1077/13186) presents similar features. In some other events the multiplicity is low not only in the fast  $\Lambda$  jet but also in the opposite one.

#### $\Xi$ Production

A practical application of  $\Lambda$  detection is a search for  $\Xi$  particles. Using  $117 \text{ pb}^{-1}$  of data, (runs 8068 thru 11472, not including FALL82) a preliminary study does show a signal (fig. 11). The cuts used are similar to those of TASSO:

- 1) require  $\Lambda$  mass to be in  $\Lambda$  peak region [1.106, 1.126] Gev
- 2) require  $\Xi$  decay distance be  $> 1.5 \text{ cm}$
- 3) construct  $E = \exp(-d/(d_{\text{perp}}))$  where  $d = \Xi$  decay distance (measured) and  $d_{\text{perp}} = E \cdot \gamma \cdot cr \cdot \sin(\theta)$  (of  $\Xi$ )
- 4) require  $0.1 < E < 0.8$
- 5) require  $|Z(\chi\Xi) - Z(\Lambda)| < 5 \text{ cm}$

The resultant signal and background (signal) =  $\Lambda\pi^-$ ,  $\bar{\Lambda}\pi^+$  and background =  $\Lambda\pi^+$ ,  $\bar{\Lambda}\pi^-$  plots are competitive with the TASSO group, and further study is planned.

Conclusions

- 1)The large amount of data accumulated and the opportunities offered by the vertex chamber, give us over the other groups the advantage of a much larger and clean  $\Lambda$  sample. This should allow us to probe the production of baryons in  $e^+e^-$  annihilations.
- 2)Results on cross-sections agrees with TASSO.
- 3)The baryon number seems predominantly conserved locally, inside one jet.
- 4)A preliminary jet analysis does not suggest a strong preference of gluon jets for  $\Lambda$ s.

References

1. Ch. de la Vaissiere; Selection of  $\Lambda$  and  $\bar{\Lambda}$  in the old and new data. TG-364, March 16, 1983.
2. Ch. de la Vaissiere; SELVEE, an easy access to  $K^0$  and  $\Lambda^0$  selection; TG-369, June 27, 1983. SELVEE is available on the G disk. A set of tapes containing events with  $K^0$  and  $\Lambda$  is also available<sup>1</sup>.
3. J.W. Dillon: VFINFP user guide (VFINDP M200C)
  - H.Schellman : VFINDP, the greatest thing Since th<sub>2</sub> sliced bread, (TG 234), March 9, 1982.
  - H.M. Schellman:  $K^0$ 's revisited, SLAC memo , July 19, 1982.
4. G.Goldhaber and J.M.Weiss; Baryon production at PEP (SLAC PUB 2810) Sept. 1981.
  - G.Goldhaber and L.Golding;  $\Lambda$  production at PEP (TG-346) Aug. 1981.
5. TASSO Collab., R. Brandelik et al, Phys. Lett. 105B (1981)75
  - S. Wu, Proceedings of the APS DPS conference, U.C., Santa Cruz, Sept. 8-11, 1981.
  - G. Wolf, Proceedings at 1982 Paris conference, C3 Journal de Physique, tome (43), 12, c3-525.
6. W. Bartel et al, Phys. Lett. 104B (1981)325.
7. Althoff et al; Z. Phys. C-Particles and Fields 17, 5-15 (1983).
8. T. Meyer, Z. Phys. C-Particles and Fields 12, 77 (1982).
9. Sau Wan Lu, proceedings of the 1982 SLAC summer institute, 555-593.
  - Sau Wan Lu and George Zobernig, Z. phys. C(Part. and Fields), 2, (1970) 107.
10. TASSO Collab. "Observation of  $\Xi \Xi$  production in  $e^+ e^-$  Annihilation" DESY 83-071, Aug. 1983.

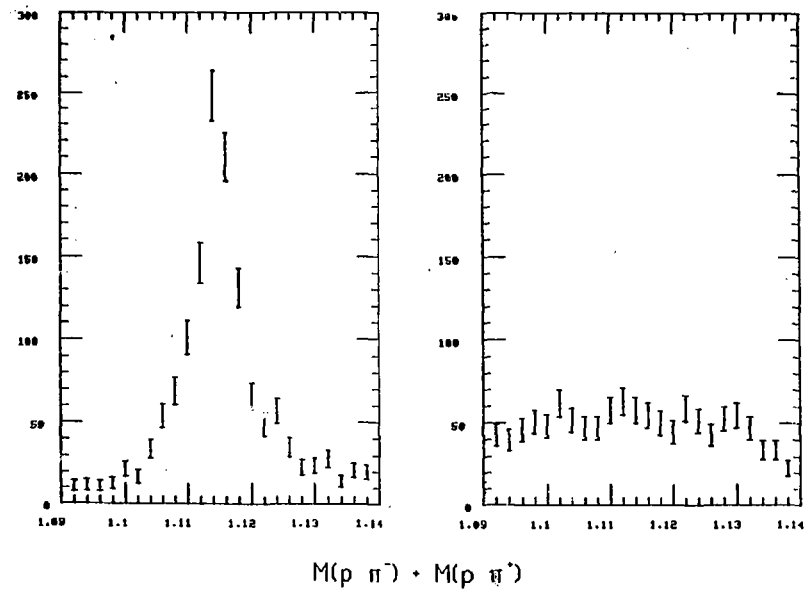


Fig.1: a)  $M(p \pi^+)$  and  $M(\bar{p} \pi^-)$  coming out of the geometrical fit to a secondary vertex : a)after all cuts; b)combinations rejected by the standard quality cut.

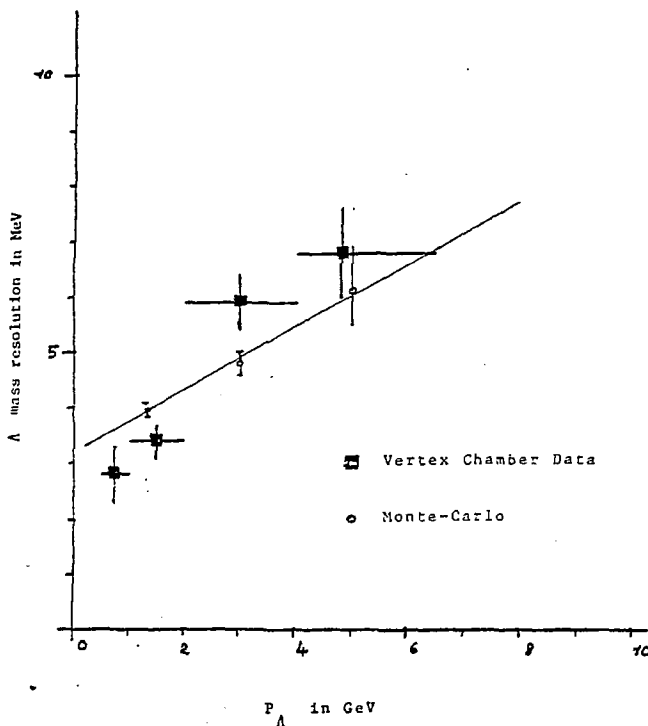


Fig.2: Variation of the  $\Lambda$  resolution (defined as  $\sigma_m$ ) with momentum.  
Data agrees with Monte-Carlo simulation.

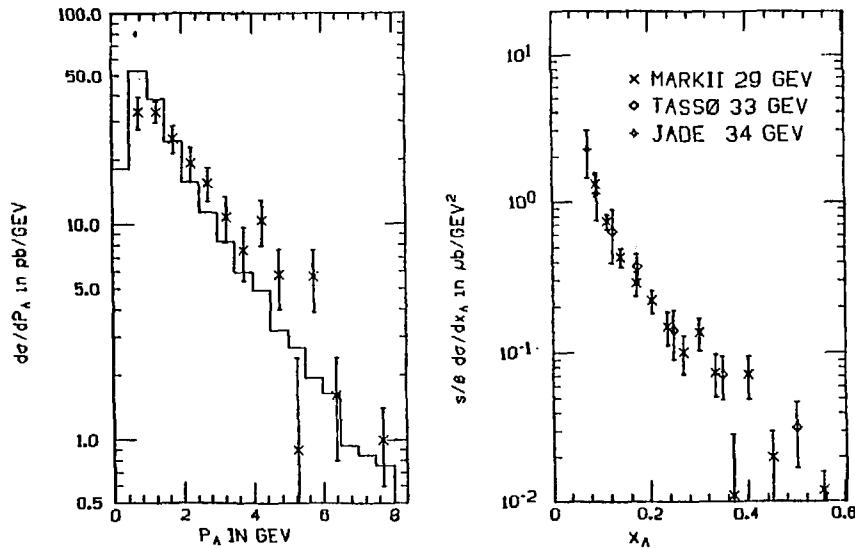


Fig.3: a)Differential cross-section  $d\sigma/dP_A$  corrected for acceptance (the errors are statistical only). Comparison with the cross-section predicted by the QCD generator(full histogram). The model has been normalized to the data by a reduction of 1.39. b)invariant cross-section  $s/\theta d\sigma/dx$  and comparison with results of TASSO and JADE. Only the data coming from the sample without drift chamber problems have been used.

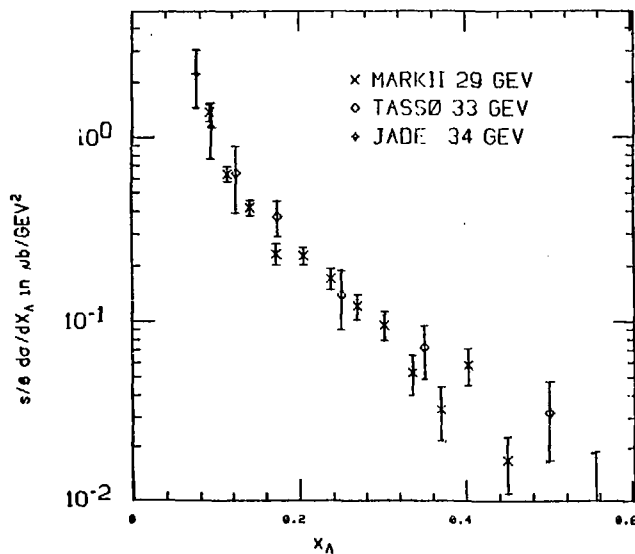


Fig.4; Same as Fig.3-b but the whole sample have been used. The events coming from the 88 pb $^{-1}$  with drift chamber problems have been given a weight 1/0.776 to compensate for the inefficiency.

ID= 263 CPD962 M(VEE) VERSUS M(VEE) + LAM ALAM +CC EVENTS

Z.E	0	1	2	3	4	5	6	7	8	9	10	11	12	13	14	
X	Y	UND1,0925,0961,1001,1041,1061,1125,1161,1201,1241,1281,1321,136	OVR&E	0												
1	X															XTOT.E 0
2	1,092	I														X 0
3	1,096	I														X 0
4	?	I														X 0
5	1,104	I														X 0
6	1,105	I														X 0
7	1,112	I					2	2	1		1					X 6
8	1,116	I					2	1	1							X 4
9	1,120	I						2								X 2
10	1,124	I														X 0
11	1,126	I									1					X 1
12	1,132	I														X 0
13	1,136	I														X 0
14	OVR	I														X 0
E	0															
XTOT.E	0	0	0	0	0	0	2	4	4	1	1	0	1	0	0	13

STATS FROM BINS, 2CALLS= 9, NTSE= 13.002  
<X>= 1.1177 +/- .127E-02, SD= .45640E-02 +/- .695E-03 FOR 1.09 < X < 1.14 (EXTREME X  
<Y>= 1.1177 +/- .177E-02, SD= .43657E-02 +/- .125E-02 FOR 1.09 < Y < 1.14 (EXTREME Y  
COR-COEF= .6746  
COVARIANCE ELLIPSE : SEMI AXES= .2957E-02 AND .7253E-02, ANGLE= 2.589 RAD

Fig.5: 2-dimensional mass plot of  $\Lambda\bar{\Lambda}$  candidates showing a clear associated production.

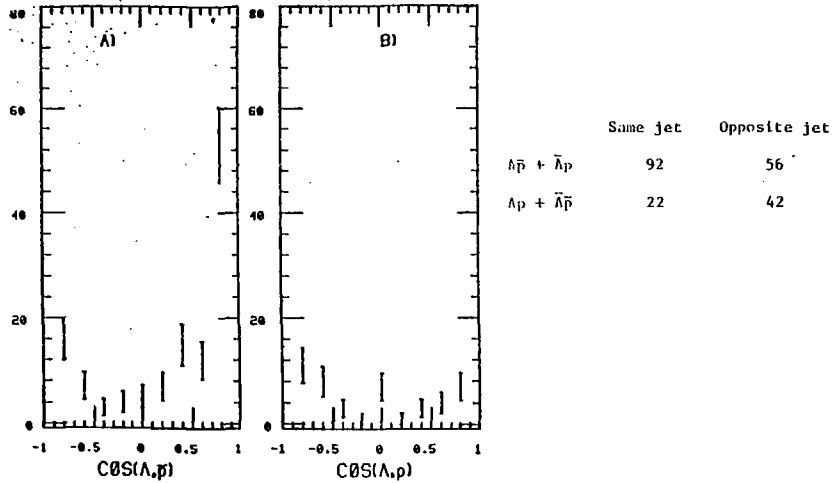


Fig.6:  
a)Cosine of the angle between  $\Lambda$  and  $\bar{p}$  (or  $\bar{\Lambda}$  and  $p$ )  
b) $\cos\theta(\Lambda,p)$  and its charge conjugate.

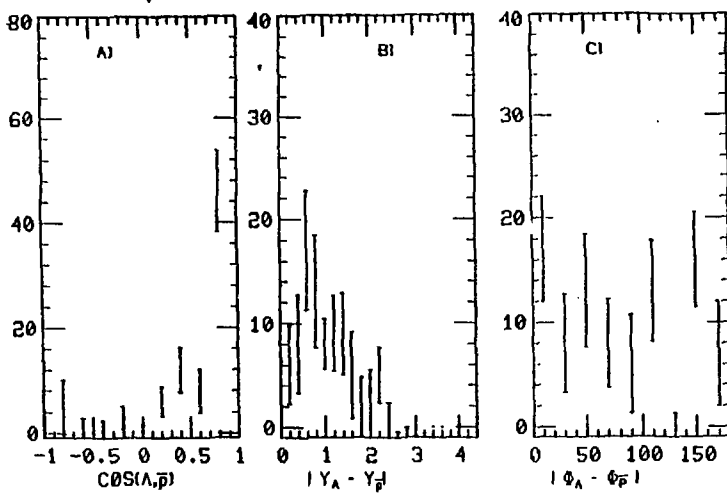


Fig.7: a)  $\cos \theta(A, \bar{p})$ , and its charge conjugate after subtraction of the contribution due to 2 baryon-antibaryon pairs. b) difference of rapidity along the sphericity axis between a  $A$  and a  $\bar{p}$  (or the charged conjugate) after subtraction of the double pair contribution. c) difference of azimuthal angles of  $A$  and  $\bar{p}$  (+c.c.), measured in the plane perpendicular to the sphericity axis. Same subtraction method.

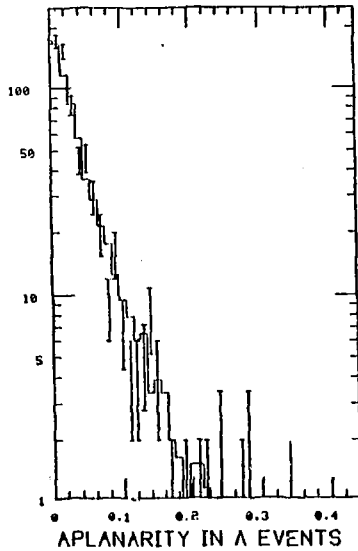
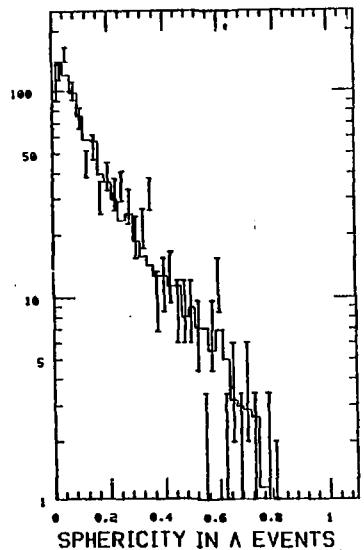


Fig.8:Sphericity and aplanarity distributions when a  $\Lambda(\bar{\Lambda})$  is required or not required(full histogram) in the event. The number of entries of the full histograms have been normalized to the number of  $\Lambda^0$ 's.

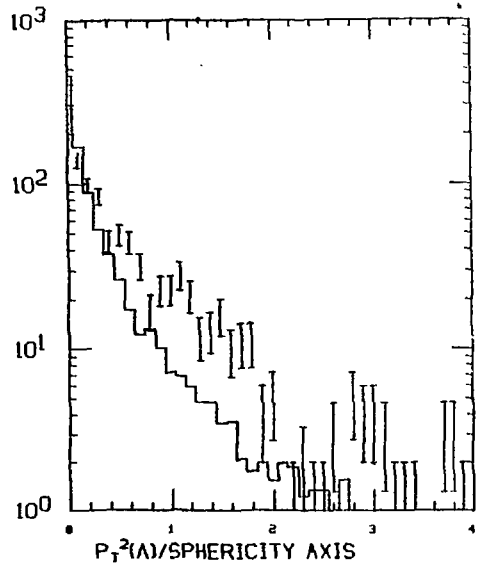
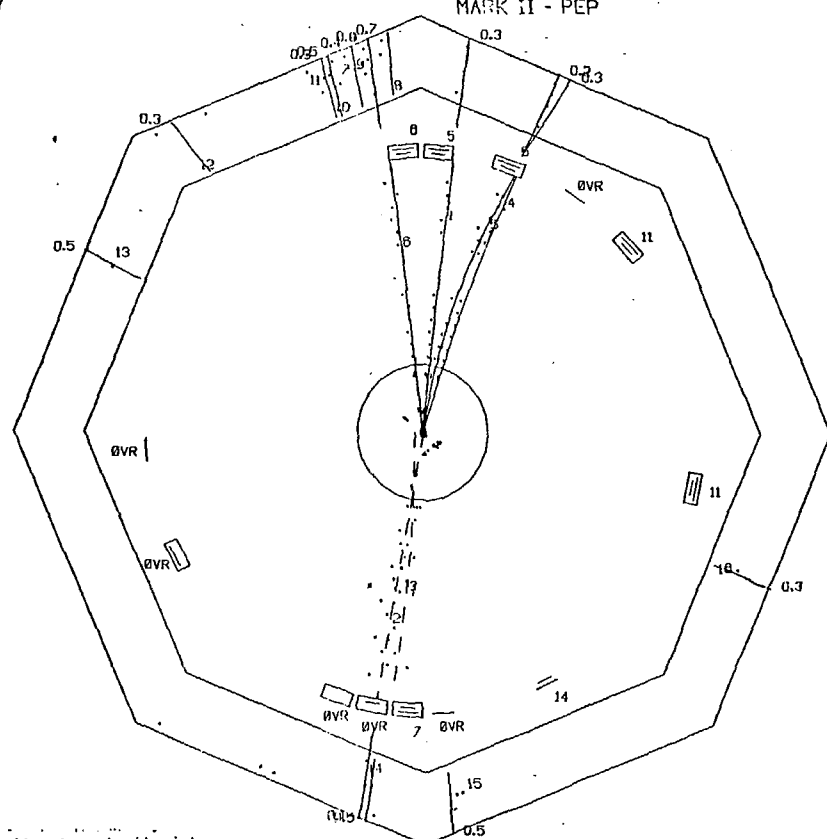


Fig.9: Comparison of the  $P_T^2(\Lambda)$  of  $\Lambda^0$ s and charged hadrons relatively to the sphericity axis in events containing  $\Lambda^0$ s. The charged distribution(full histogram) has been normalized to the number of  $\Lambda^0$ s.

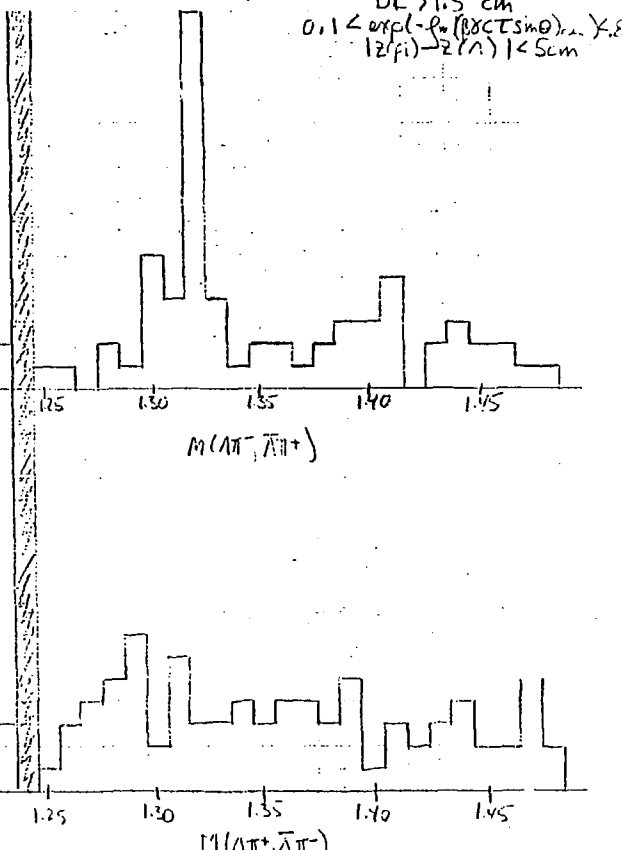
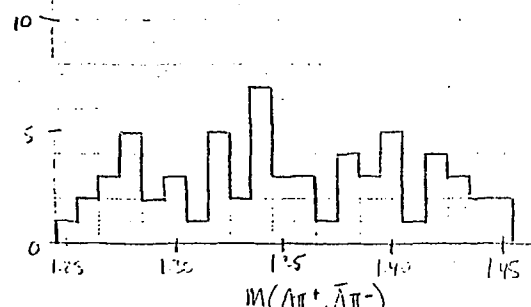
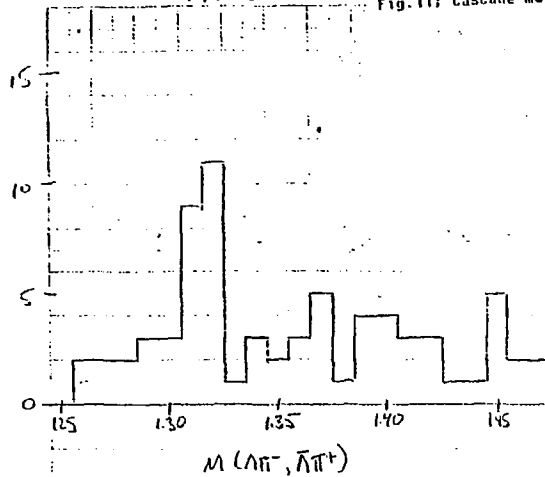
## TRIGGER 84F V

TRK P	EL	TBT ID
1	3.4	0.1 PI+
2	0.0	0.1 PI-
3	0.8	PI+
4	0.9	0.2 PI+
5	0.3	0.3 PI+
6	3.0	0.0 PI-
7	0.4	G
8	0.7	G
9	0.4	G
10	0.5	G
11	0.3	G
12	0.3	G
13	0.5	G
14	0.5	G
15	0.5	G
16	0.3	G

Fig. 10: Example of a fast  $\bar{\Lambda}$  practically alone in its jet.

TASSO

Fig. 11: Cascade mass plots of MARK2 and TASSO  $M/\pi\pi K2$

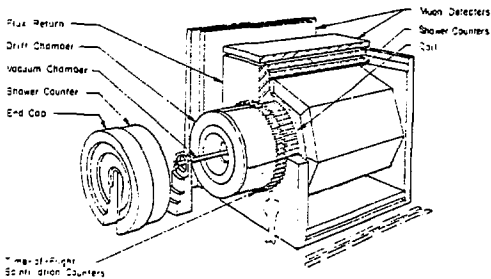
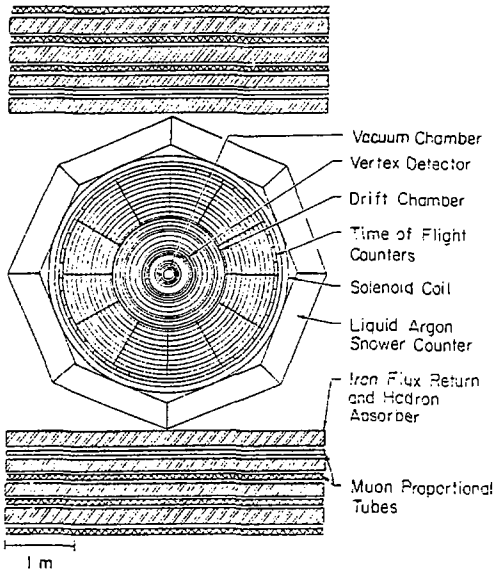


ANNEXE 1 : Description sommaire du détecteur MARK II

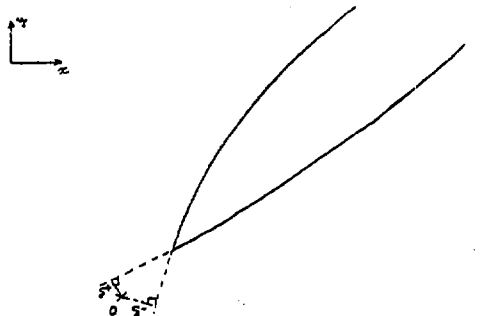
MARK II

LOCATION	PEP e <sup>+</sup> e <sup>-</sup> storage ring SLAC, Stanford, CA, USA
MAGNET	4.6 kG Al coil solenoid, 1.5 m radius (currently running at 2.3 kG)
TRACKING	Central drift chamber: Active length = 2.64 m, inner radius = 0.41 m, outer radius = 1.45 m 6 axial layers, 10 stereo layers ( $\pm 3^\circ$ ) 50% ethane, 50% argon $\sigma \approx 200 \mu$ Vertex drift chamber: Cylindrical drift chamber, 1.2 m long, inner radius = 10 cm, outer radius = 35 cm Only axial wire layers (4 near $r = 12$ cm, 3 near $r = 30$ cm) $\sigma \approx 100 \mu$ Be beam pipe (0.006X <sub>0</sub> ) Combined $(\Delta p/p)^2 = (0.015)^2 + (0.01p)^2$ Tracks extrapolated to interaction point within 100 $\mu$
SHOWER COUNTERS	8 modules of Pb-liquid argon (15X <sub>0</sub> each), arranged in octagon outside coil Covers 64% of 4 $\pi$ 2 mm Pb sheets separated by 3 mm liquid argon gaps 37 layers (0.4X <sub>0</sub> sampling) are ganged to provide 9 samples in depth Readout in 1.3 cm wide strips in $\phi$ , $\theta$ , $\eta$ , $\phi$ directions $\Delta E/E = 13\%/\sqrt{E}$
TIME OF FLIGHT	48 scintillation counters read out at both ends Cover 75% of 4 $\pi$ 1.50 m flight path at $\theta = 90^\circ$ , $\sigma = 340$ ps K, $\pi$ separation up to 1.35 GeV/c at 1 $\sigma$ level
END CAPS	2 layers Pb-proportional chamber (5X <sub>0</sub> ) with 4 successive cathode strip readouts ( $\theta$ , $\phi$ , R-spiral, L-spiral) 50% argon, 50% ethane
MUON DETECTION	Proportional tubes interleaved with steel absorber (4 layers each for total thickness of 1 m) covering 55% of 4 $\pi$
SMALL ANGLE TAGGING LUMINOSITY MONITOR	6 planar drift chambers followed by shower counters Octagonal shower counters cover 32 mrad $< \theta <$ 80 mrad contain 18 layers 1/4" Pb and 1/2" scintillator, read out with BBQ wave shifter, front 5 layers separately from back 13 $\Delta E/E = 15.5\%/\sqrt{E}$ 3 sets of scintillation counters
REFERENCES	<ol style="list-style-type: none"><li>1. G.S. Abrams et al., Phys Rev. Lett. 43 (1979) 477, and <i>ibid</i> 481.</li><li>2. W. Davies White et al., Nucl. Instr. &amp; Meth. 160 (1979) 227.</li><li>3. G.S. Abrams et al., IEEE Trans. Nucl. Sci. NS 25 (1978) 1, <i>ibid</i> 309, and NS 27 (1980) 59.</li><li>4. J.A. Jaros, Proc. Int. Conf. on Instrumentation for Colliding Beam Physics, SLAC-250 (1982).</li></ol>

## MARK II



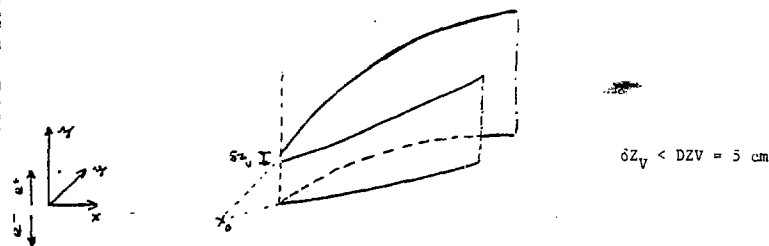
1) distance d'approche maximum



$$S^+ > DCPR = 2 \text{ mm}$$

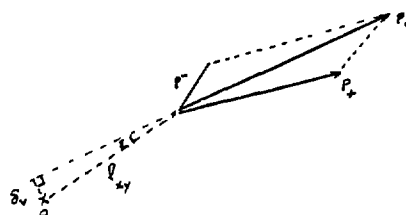
$$S^- > DCPI = 1 \text{ mm}$$

2) Point de rencontre dans l'espace



$$\delta Z_V < DZV = 5 \text{ cm}$$

3) Alignement du  $V_0$



$$\delta_{V_0} = l_{xy} \sin \epsilon < RSNV = 5 \text{ mm}$$

$$ct = \frac{l_{xy}}{By \cos \theta} > CTLM = 4 \text{ ms}$$

Illustration des critères géométriques de sélection des A

ANNEXE 2

VFINDP : VFINDP est un ensemble de programmes destiné, comme son nom l'indique, à reconnaître des vertexs secondaires du type  $V^0$ . VFINDP fonctionne comme une boîte noire. À l'entrée un "menu" d'options et de critères de sélection, à la sortie des candidats  $V^0$  satisfaisant ces critères.

Essentiellement VFINDP associe toutes les paires de traces positives et négatives satisfaisant un certain nombre de ces critères. Des hypothèses de masses sont alors assignées aux 2 traces. Celles-ci sont ajustées à un vertex secondaire qui doit satisfaire à d'autres critères pour être retenu comme  $V^0$ .

Les critères choisis pour cette étude suivent de près la définition d'un  $V^0$ .

- 1) Les deux traces doivent manquer le point d'interaction primaire. Le test est effectué sur la projection perpendiculaire à l'axe du faisceau qui est la plus précise. On mesure la "distance d'approche.maximum" des traces au point d'interaction. Cette opération nécessite une extrapolation. Grâce à la chambre de haute précision, cette extrapolation est très précise :  $100 \mu$  .
- 2) Les deux traces doivent se rencontrer dans l'espace. Malheureusement l'im-précision le long de l'axe du faisceau ne permet pas d'être sélectif.
- 3) Les 2 traces sont ajustées à provenir d'un même vertex secondaire. Le test de l'ajustement doit être positif.
- 4) La ligne de vol du  $V^0$  et la somme des impulsions sont assujettis à être alignés.
- 5) Les très courts parcours sont éliminés. Plutôt que sur le parcours, le test est effectué sur le temps de vol propre  $\tau = \lambda/B\gamma$  .
- 6) La masse du  $V^0$  doit être compatible avec celle d'un  $K^0$ ,  $\Lambda$  ou  $\bar{\Lambda}$ .

### Qualité d'un V

De façon à améliorer la pureté de l'échantillon de  $K^0$ ,  $\Lambda$ ,  $\bar{\Lambda}$ , nous avons introduit la notion de qualité d'un  $V^0$ , ce qui permet ensuite de faire une coupure sur cette qualité.

La Fig. 1 du rapport montre la présence d'un fond sous le signal du  $\Lambda/\bar{\Lambda}$ . Ce fond est du à des paires de traces qui simulent un  $V^0$  où à un  $K^0$  mal identifié.

La séparation du signal et du fond est basée sur l'analyse multi-dimensionnelle Si l'on considère les quelques caractéristiques d'un  $V^0$  sur lesquelles est basée la sélection, le comportement paraît souvent sensiblement différent entre le fond et le signal, pas assez cependant pour permettre une séparation très propre.

Le principe de la méthode est de combiner toutes ces caractéristiques à l'intérieur d'une variable unique, la qualité, dont le pouvoir de séparation est plus fort. Dans la qualité, nous avons introduit l'information sur l'identification des secondaires par "temps de vol". Cette information étant souvent insuffisante et pas toujours disponible n'avait pas été utilisée au niveau de VFINDP.

L'extrait ci-dessus de la Réf. 2, détaille le calcul de la qualité d'un  $V^0$ .

### Definition of $K^0$ and $\Lambda$ quality.

3 types of ingredients enter in determining the  $V$  quality.

-Time of flight compatibility of secondaries. The time of flight probability, which is mainly useful for slow  $\Lambda$ s, reflects the discrepancy between the measured time of flight (when available or significant) and expected time of flight.

-Geometrical quantities: DSV(Match in z of the 2 secondaries at the XY intersection), RSHV(distance of closest approach of the  $V$  line of flight), SUMDCA ( $\sqrt{(\sum \text{distance of cl. appr. of secondaries squared})}$ ), COSTAR (Cos. of the decay angle/line of flight in the  $V$  frame). For these factors, we estimated the probability from the histograms of these quantities  $PK(I)$  and  $WI(I)$  in the peak and wings regions. (This histograms are entered numerically in the function PROZY). The probability factor is essentially  $PK(I)/WI(I)$  normalized to a convenient factor. The fig.1 shows these distributions for  $VC$  data. They are found generally independent from the type of data or  $V$ .

-Penalties and bonuses. Penalties and bonuses occurs when secondaries of a  $V$  that decays outside the  $VC$  inner layer have unwanted (or no) hits in these layers. A penalty is also given to a  $\Lambda$  candidate when a secondary is labelled electron in the liquid argon (Function IDGA). This allows to kill pair contamination. Penalties and bonuses are empirical.

SQUAL is actually the logarithm of the product all these probability factors. The Fig.2 and 3 show the cumulated distribution of the quality of candidates  $K^0$ ,  $\Lambda^0$  in the peak and wings regions. The standard probability cuts (QUALOW and UPQUAL in the common VSELECT), divide the quality distribution in 3 zones: 1)The low quality region that is mostly background; 2)The high quality region with low background; 3)The upper quality region virtually background free but with some loss of signal.

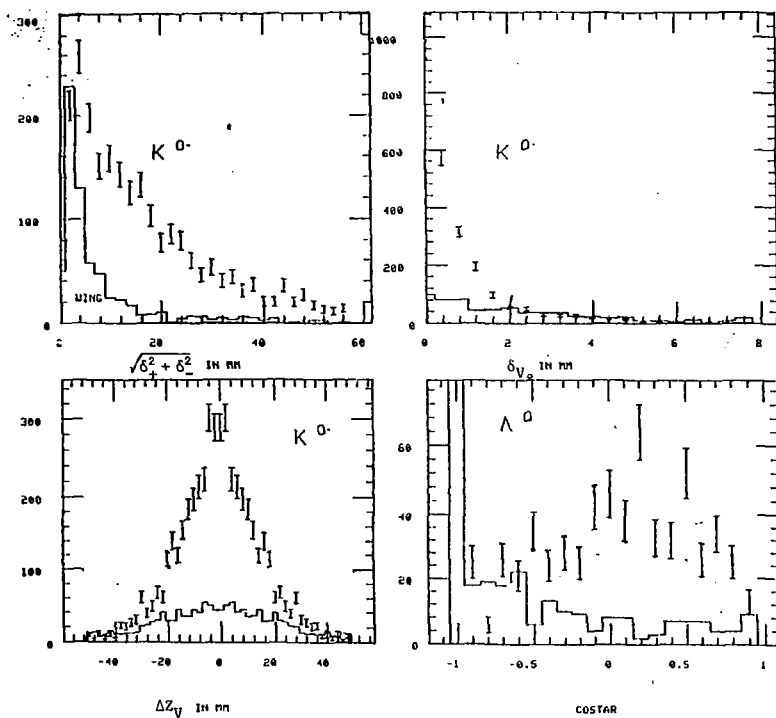


Fig.1:Distributions of the geometrical or dynamical variables. These distributions are shown for the V peak and wings regions (full histogram). The peak contribution is estimated through a linear peak minus wings subtraction. Whenever the distribution differs significantly between  $K^0$  and  $\Lambda^0$  or data type, it may be entered separately in the function PRUVZ.

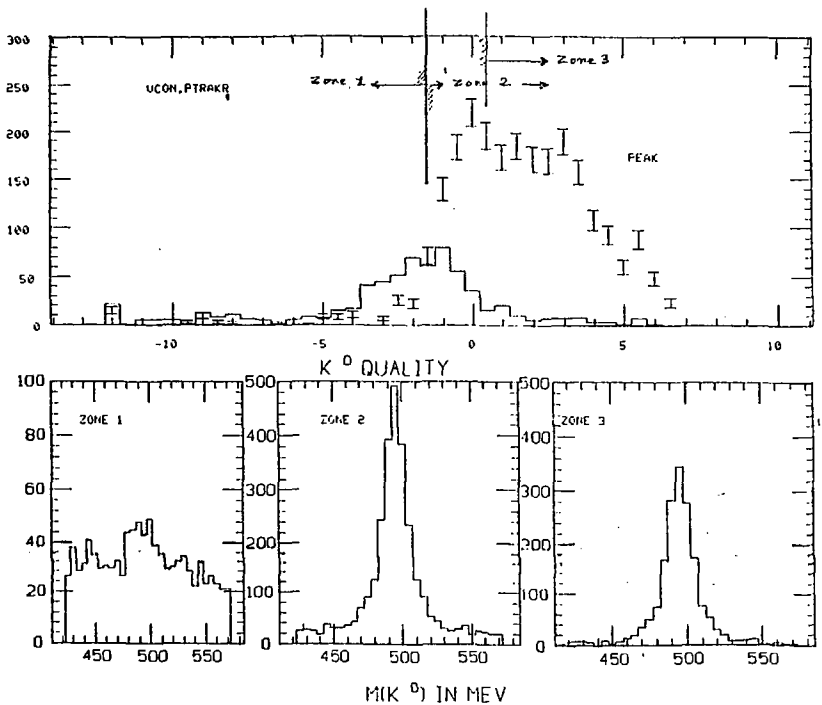


Fig.2: $K^0$  probability distribution for vertex chamber data. in the peak and wings regions. The default probability cuts QVAL010 and UPVAL01 are indicated, and the lower part of the figure shows the  $K^0$  mass spectrum in the 3 zones that can be defined. Solid histograms are combinations of low QVAL that are cut.

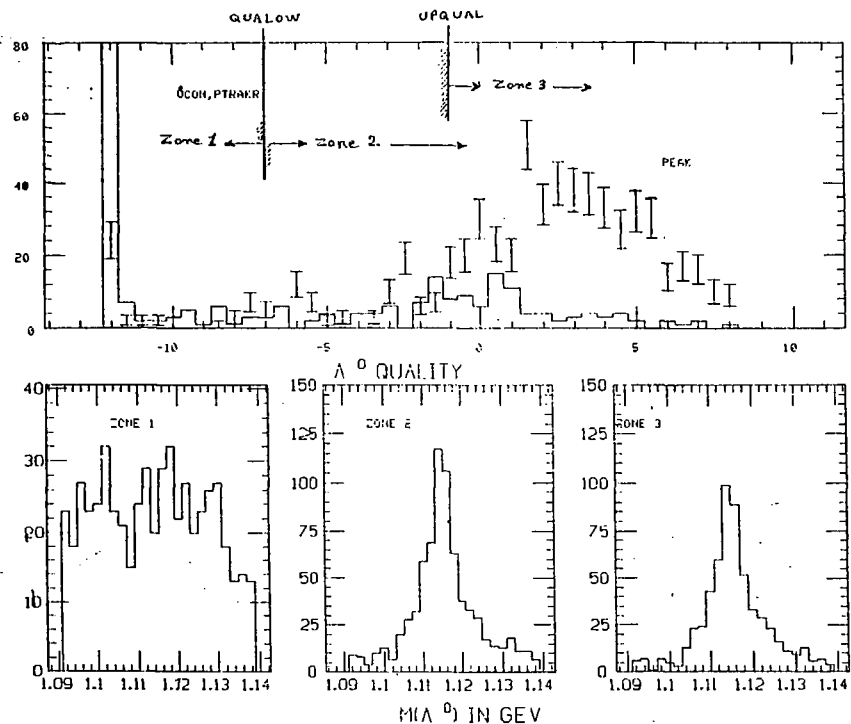


Fig.3: Same as Fig.2 but for  $A^0$  s.